Electronic supplementary material

Ultrathin cobalt phosphide nanosheets as efficient bifunctional catalysts for water electrolysis cell and the origin for cell performance degradation

Jinfa Chang,[a,b] Liang Liang,[b] Chenyang Li,[b] Minglei Wang,[b] Junjie Ge,[b] Changpeng Liu[b,] and Wei Xing[a,b,*]*

[a] State Key Laboratory of Electroanalytical Chemistry, Changchun Institute of Applied Chemistry, Chinese Academy of Sciences, Changchun 130022 (P.R. China)

E-mail address: xingwei@ciac.ac.cn (W. Xing)

[b] Laboratory of Advanced Power Sources, Jilin Province Key Laboratory of Low Carbon Chemical Power Sources, Changchun Institute of Applied Chemistry, Chinese Academy of Sciences, Changchun 130022, PR China;

E-mail: liuchp@ciac.ac.cn (C. Liu)

Experimental Section

Materials: Sodium hypophosphite monohydrate (≥ 99.0%, $NaH_2PO_2 \cdot H_2O$), cobalt nitrate hexahydrate (≥ 98.0%, $Co(NO_3)_2 \cdot 6H_2O$), iridium oxide nanoparticles (IrO_2) and urea ($CO(NH_2)_{2)}$ were purchased from Aldrich Chemical Co. (USA). Vulcan carbon powder XC-72 (denoted as carbon) was purchased from Cabot Co. (USA). Nafion solution (5%) and PTFE (10%) was purchased from Dupont Co. (USA). Potassium hydroxide (≥ 95.0%, KOH) and ethanol (≥ 99.7%) were purchased from Beijing Chemical Co. (China). All the chemicals were of analytical grade and used as received. Highly purified N_2, O_2, and O_2/ N_2 (O_2, 1.0 mol %) were supplied by Changchun Juyang Co Ltd. Ultrapure water (resistivity：$\rho \geq 18$ MΩ cm^{-1}) was used to prepare the solutions.

Synthesis of CoP NS

The CoP NS was synthesized as described in Ref. [1] with slightly modification. Specifically, the CoP NS was prepared as follows: 2 mmol $Co(NO_3)_2 \cdot 6H_2O$ was dissolved in 160 mL water and subsequently heated to 80 °C under magnetic stirring. Then, 22 mL of 8 M NaOH was added to the solution. After stirring for 10 min, the precipitate was collected and dried, followed by centrifuging and washing with water for several times, then the Co_3O_4 NS was obtained. To prepare CoP NS, Co_3O_4 NS and $NaH_2PO_2 \cdot H_2O$ were placed at two separate positions in one closed porcelain crucible with $NaH_2PO_2 \cdot H_2O$ located at the upstream side of the furnace. The molar ratio for Co to P was 1:5. Subsequently, the samples were heated to 300 °C and rest at the temperature for 2 h under a static N_2 atmosphere. After the heat treatment, the oven was later cooled to room temperature under the protection of flowing N_2. Finally, the CoP NS was passivated in a 1.0 mol % O_2/ N_2 mixture at 20 mL min^{-1} for 3 h at room temperature.

The equation for the formation of CoP is shown as follows:

$$12Co_3O_4 + 69\ NaH_2PO_2 \rightarrow 36\ CoP + 23Na_3PO_4 + 10H_3PO_4 + 6H_2O.$$

To complete the reaction, a molar ratio at approximately 1:2 between Co and P precursors is needed. When the temperature was higher than 200 °C, the decomposition of NaH_2PO_2 occurs as a side reaction. Therefore, to ensure the complete conversion of Co_3O_4 NS into CoP NS, excessive NaH_2PO_2 was needed. Hence, molar ratio at 1:5 for Co:P precursors was selected. In fact, molar ratio at 1:5 was used widely in the

synthesis of CoP, as suggested in literature[1, 2]. During the reaction, the NaH_2PO_2 may decompose and release P containing molecule (PH_3). In order to restrain PH_3, excessive cupric sulfate solution ($CuSO_4$) was used at the stern of tube furnace to convert PH_3 into H_3PO_4. The reaction can be express as follows:

$$4CuSO_4 + PH_3 + 4H_2O \rightarrow 4Cu\downarrow + H_3PO_4 + 4H_2SO_4$$

As a result, the noxious gas is transformed into H_3PO_4 before entering into the atmosphere. Therefore, we claim that the CoP NS was synthesized using a simple and green approach.

Physical characterizations

AFM images were obtained with a Veeco Dimension 3100 instrument with a silicon cantilever operated in tapping mode. Scanning electron microscopy (SEM) measurements were performed with an XL 30 ESEM FEG field emission scanning electron microscope. Transmission electron microscopy (TEM), high resolution transmission electron microscopy (HR-TEM), Fast Fourier Transformation analyzer (FFT), high-annular dark-field scanning transmission electron microscopy (STEM) and element mapping analysis were conducted on Philips TECNAI G2 electron microscope operating at 200 kV. X-ray diffraction (XRD) measurements were performed with a PW-1700 diffractometer using a Cu K_α (λ=1.5405 Å) radiation source (Philips Co.). The textural and morphological features of the CoP NS were determined by nitrogen physisorption at 77 K in a Micromeritics ASAP 2020. Textural properties such as the specific surface area pore volume and pore size distribution were calculated from each corresponding nitrogen adsorption−desorption isotherm, applying the Brunauer−Emmett−Teller (BET) equation and the Barrett−Joyner−Halenda (BJH). X-ray photoelectron spectroscopy (XPS) measurements were carried out on Mg K_α radiation source (Kratos XSAM-800 spectrometer).The bulk compositions were evaluated by inductively coupled plasma optical emission spectrometer (ICP-OES, X Series 2, Thermo Scientific USA). In order to probe and compare the electrical resistance of IrO_2 and CoP, a typical four-probe method (performed on KDY-1-type four-probe resistivity/square resistance tester, Guangzhou KunDe Co., Ltd. China) was used and measurements at ambient temperature (ca. 25 ^oC). The powder samples were pressed into pellets with a diameter of 10 mm and a thickness of about 3 mm under a pressure of $4.9x10^8$ Pa. Each sample was test five times and the average value was used.

It should be noted that all the products were saved in vacuum oven at 25 ^{o}C. Due to the same result of intermediate product to Ref [1], we didn't show the XRD, TEM and SEM characterization of intermediate Co_3O_4 NS here.

Electrochemical measurements

Electrochemical measurements were performed with EG & G PARSTAT 4000 potentiostat/galvanostat (Princeton Applied Research Co., USA). A conventional one-component three-electrode cell was used, including a glassy carbon electrode (GCE, geometric area = 0.07 cm^2) as the working electrode, a platinum foil was used as the auxiliary electrode and a mercuric oxide (Hg/HgO, 1 M KOH) electrode was used as the reference electrode. To prepare the working electrode, 5 mg of the catalyst and 100 μL of 5 wt% Nafion solution were dispersed in 900 mL of ethanol solvent, followed by ultrasounded at least 30 min. Then 10 μL of the ink was dropped onto a GCE (~loading: 0.71 mg cm^{-2}). In order to enhanced the electroconductibility of CoP NS, physical mixing CoP NS with carbon (mass ratio, 1:1) was employed. The electrolyte (1 M KOH) was degassed by bubbling O_2 for at least 30 minutes before the electrochemical measurements. Prior recording the OER activity of CoP NS, the catalysts were activated by 20 CV scans along the potential window of 0.3 to 0.9 V vs. Hg/HgO in 1 M KOH at a scan rate of 100 mV s^{-1}, then the linear sweep voltammetry (LSV) with a scan rate of 5 mV s^{-1} was performed in a range from 0.3 to 0.9 V vs. Hg/HgO. During electrochemical experiments, the electrolyte was agitated using a magnetic stirrer rotating at 300 rpm. Durability test was then carried out by cyclic voltammetry (CV) scanning from 0.35 to 0.85 V vs. Hg/HgO for 1000 cycles at a scan rate of 100 mV s^{-1}. The durability of CoP NS/C was also investigated through chronopotentiometry, the time-dependent voltage was recording under a static current density of 10 mA cm^{-2} for 24 hours. The electrochemical impedance spectroscopy (EIS) measurements were carried out from 100000 to 0.1 Hz in 1 M KOH. In all measurements, Hg/HgO was used as the reference, and all the potentials reported in our work were vs. the reversible hydrogen electrode (RHE). In 1 M KOH (pH = 13.61), E(RHE) = 0.098 + 0.059*pH. Ohmic drop was corrected using the current interrupt method.

The generated gas was confirmed by gas chromatography analysis and measured quantitatively using a calibrated pressure sensor to monitor the pressure change in the anode compartment of a H-type electrolytic

cell. The glass carbon sheet (1*2 cm) was used as working electrode with a catalysts loading of 0.71 mg cm^{-2}. The Faradaic efficiency was calculated by comparing the amount of measured oxygen with calculated oxygen generated at a constent oxidative current of 10 mA cm^{-2} in 1 M KOH for 100 min electrolysis (assuming 100% FE). Pressure data during electrolysis were recorded using a CEM DT-8890 Differential Air Pressure Gauge Manometer Data Logger Meter Tester with a sampling interval of 1 point per second.

Prior to the use of titanium felt (Alfa Aesar, porosity 95%, purity 95%) as catalyst support, the titanium felt were pretreated in acetone, ethanol for 1 hour respectively and were rinsed with deionized water thoroughly. To evaluate the bifunctionality of CoP NS in alkaline solutions, the catalyst was first dispersed in ethanol, and the suspension was loaded on two 1*2 cm titanium felt sheet. The loading on both anode and cathode was at 0.71 mg cm^{-2}. To ensure the binding between the catalyst and the titanium felt sheet support, 1.5 mL of PTFE (10%) was dropped onto each electrode, after which the titanium felt sheet was heat treated at 250 ^{o}C for 1 hour. The LSV experiments were performed with a potential window range from 0.5 to 1.8V at a scan rate of 5 mV s^{-1} in 1 M KOH. The stability of the electrolyzer was examined using galavanostatic experiments in the same electrolyte. The current density was kept constant at 10 mA cm^{-2} over 24 hours of electrolysis.

Fabrication of membrane electrode assembly (MEA) with catalyst-coated substrate (CCS) method

The MEA was prepared according to the Reference[3]. CoP NS was used both as anode catalyst for oxygen evolution reaction (OER) and as cathode catalysts for hydrogen evolution reaction (HER). The untreated carbon paper (TGPH#90, Toray Inc., Japan) and titanium (Ti) foam were employed as anode and cathode gas diffusion layer (GDL), respectively. A YAB membrane (Foma Corporation, Germany) with a thickness of 0.13~0.15 mm was used as anion exchange membrane (AEM). The catalysts were mixed with deionized water, isopropanol and PTFE ionomer suspension (10 wt % polymer in suspension) to obtain well dispersed ink using magnetic stirring combined with ultrasonication. The as prepared ink was coated onto the surface of Ti foam and Toray TGP90 plain carbon paper using a spray gun to obtain a CCS for both anode and cathode. The binder content (10 wt% PTFE ionomer) was at approximately 5 wt% polymer for

both anode and cathode catalysts layer. The catalysts loading was controlled at 5 mg/cm^2 for the anode and cathode catalysts layer. The catalyst-coated substrate was heat treated at 250 ^{o}C for 1 hour. The size of all electrode catalysts layer was $\pi\times$ 2 cm × 2 cm (i.e. 12.56 cm^2 active areas). Anode CCS, YAB membrane and cathode CCS were assembled together in the cell hardware to form an MEA (See Fig. S 9). For comparison, a water electrolysis cell with Pt black as cathode catalyst and IrO_2 as anode catalyst was selected as the 'reference' MEA, the catalyst loading, gas-diffusion electrodes, membrane, preparation technology and the test condition of the 'reference' MEA are all same to the bifunctional CoP NS catalyst.

Cell performance evaluation

The water electrolysis cell setup is shown in Fig.. S9, which was used to evaluate the performance and durability of the single water electrolysis cell (See Fig. S 9b and 9c). Cell potential and current was controlled through an Arbin testing system (Arbin Instruments, United States). 1 M KOH was supplied into anode chamber at a flow rate of 5 mL min^{-1} with a peristaltic pump (BT100-2J, LongerPump Co. China). The cell temperature was maintained at 50 °C. Before the polarization measurements, the electrolysis cell was pretreated at 100 mA cm^{-2} for 4 h to activate the catalyst layer. The polarization curves (current density vs. cell voltage) were obtained using the Arbin testing system in galvanodynamic mode, i.e., the steady-state polarization curve was measured by recording the cell potential for 1 min from the circuit voltage under constant current density. For the durability tests, a constant current of 300 mA cm^{-2} was applied onto the electrolysis cell, and the cell voltage as a function of test time was recorded by Arbin testing system. Before the durability tests, resistance was monitored by a milliohm meter (Agilent 4338B, United States), the polarization curve was corrected with i-R drop.

In order to investigated the origin of cell degradation, the sample after electrolysis was collected by scraping off the surface layer from the carbon paper or Ti foam with a sharp knife. The XRD, SEM, TEM, XPS were performed afterward.

Table S1. Summarize the elements contents of the CoP NS.

	elements content					
element	Co[a]	P[a]	O[a]	Co[b]	P[b]	O[b,c]
Wt (ppm)	-	-	-	650100	324600	25300
Wt. %	-	-	-	65.01	32.46	2.53
At. %	47.61	38.03	14.36	47.77	45.38	6.85

a. Derived from XPS;

b. Derived from ICP-OES.

c. When we analysis the element content using ICP-OES, the testing sample undergoes high temperature fusion and dissolution process in water. Hence, a list of non-metal elements, such as H, C, N, O, F and so on, cannot be detected. Furthermore, it is shown that it is harder to excite the non-metal elements (such as H, C, N, O, etc.) into the excited state due to the high electron negativity. However, the emission spectra (transition from excited states back to the ground state) of these elements locate in the far infrared region, which is not within ICP-OES spectra range. Therefore, generally speaking, elements including H, C, N, O, etc. cannot detected by ICP-OES. If we hypothesize that only Co, P and O three elements were present in the sample, then, the content of O element can be calculated through 100% - Co% - P%. Therefore, in order to measure the O content in the sample, we repeated the tests through ICP-OES. The elements content (wt %) were calculated through the X/M*100%, where X is the content of Co and P, respectively, while M is the total weight of sample. As shown in Table S1, the elements content (at%) of Co, P and O is 47.77%, 45.38% and 6.85%, in sequence. These results are consistent with the XRD result where only partially surface passivation was observed.

Table S2. Comparison of OER activities of CoP NS/C catalysts with recently publication in alkaline conditions (The current density of 10 mA cm^{-2} was chosen because it represents the current density from a device with 12% solar to hydrogen efficiency, which is at the upper end of a realistic device[4]).

Materials	Overpotential @ 10 mA cm^{-2}	Electrolyte (M, KOH)	References
CoP NS	361	1	
CoP NS/C	277	1	This work
IrO_2	320	1	
IrO_2	320	0.1	[5]
IrO_2-CNT	360	1	[6]
g-C_3N_4 NS-	370	1	
CoOx@CN	410	1	[7]
NiOx	360	0.5	[8]
Ni-Co_2-O	362	1	[9]
Co_3O_4/graphene	310	1	[10]
N-CG-CoO	340	1	[11]
Co_3O_4C-NA	290	1	[12]
CoMn-LDH	324	1	[13]
NiCo-LDH	367	1	[14]
$NiCo_2O_4$	565	1	[15]
NiFe-LDH	320	1	[16]
Co_3O_4/2.7Co_2MnO_4	540	0.1	[17]
α-Fe_2O_3 NA/CC	420	1	[18]
$Mn_{0.1}Ni_1$	420	0.1	[19]
3D NF/PC/AN	407	1	[20]
CoP NP	340		
CoP NR	320	1	[21]

Table S3 Comparison of HER activities of CoP NS/C catalysts with recently publication in alkaline conditions.

Materials	Overpotential (V)	@ XX mA cm^{-2}	Tafel slope (mV dec^{-1})	Electrolyte (M, KOH or NaOH)	References
CoP NS/C	0.111	10	70.9	1	This work
	0.139	20			
PCPTF	0.430	30	N.A.	1	[22]
NiS_2 NA/CC	0.149	10	104	1	[23]
Ni_3S_2/Ni foam	0.123	10	110	1	[24]
NiSe/NF	0.096	10	120	1	[25]
Ni_2P	0.220	10	N.A.	1	[26]
WN NA/CC	0.285	10	170	1	[27]
Ni_5P_4	0.150	10	N.A.	1	[28]
Mn_1Ni_1	0.420	20	N.A.	0.1	[19]
Ni_5P_4	0.049	10	98	1	[29]
Ni_2P	0.069		118		
CoO_x@CN	0.232	10	N.A.	1	[7]
N-Co@G	0.337	10	N.A.	0.1	[30]
Co-NRCNTs	0.450	20	N.A.	1	[31]
CoP/CC	0.209	10	129	1	[32]
C_3N_4/TiO_2	0.300	1.3	N.A.	0.1	[33]
WP NAs/CC	0.150	10	102	1	[34]
FeP NAs/CC	0.218	10	146	1	[35]
NiO/Ni-CNT	0.125	20	82	1	[36]
Ni_2P–G@NF	0.150	20	30	1	[37]
np-CoP/Ti	0.150	20	71	1	[38]

Table S4 Compare the binding energy and elemental content for Co 2p, P 2p and O 1s of the fresh prepared CoP NS with the CoP NS that after electrolysis on cathode HER side and anode OER side. (The elemental content was obtained by deconvolution the Co, P and O singal)

	Co 2P $_{3/2}$	Co_3O_4 2p $_{3/2}$	Co_3O_4 satellite	Phosphide		orthophosphate		Lattic O	Adsorbed O
Fresh prepared CoP	36.73% 777.4 eV	63.27% 780.9 eV	--	66.67%		33.33%		71.39% 531.4 eV	28.61% 532.9 eV
				129.8 eV	130.9 eV	133.3 eV	134.4 eV		
After HER electrolysis side of CoP	73.49% 777.3 eV	26.51% 780.8 eV	--	61.09%		38.91%		62.45% 531.1eV	37.55% 532.6 eV
				129.7 eV	130.8 eV	133.2 eV	134.3 eV		
After OER electrolysis side of CoP	25.10% 778.6 eV	58.03% 782.1 eV	16.87% 786.4 eV	22.28%		77.72%		65.99% 531.0 eV	34.01% 532.5 eV
				129.1 eV	130.2 eV	133.0 eV	134.3 1 eV		

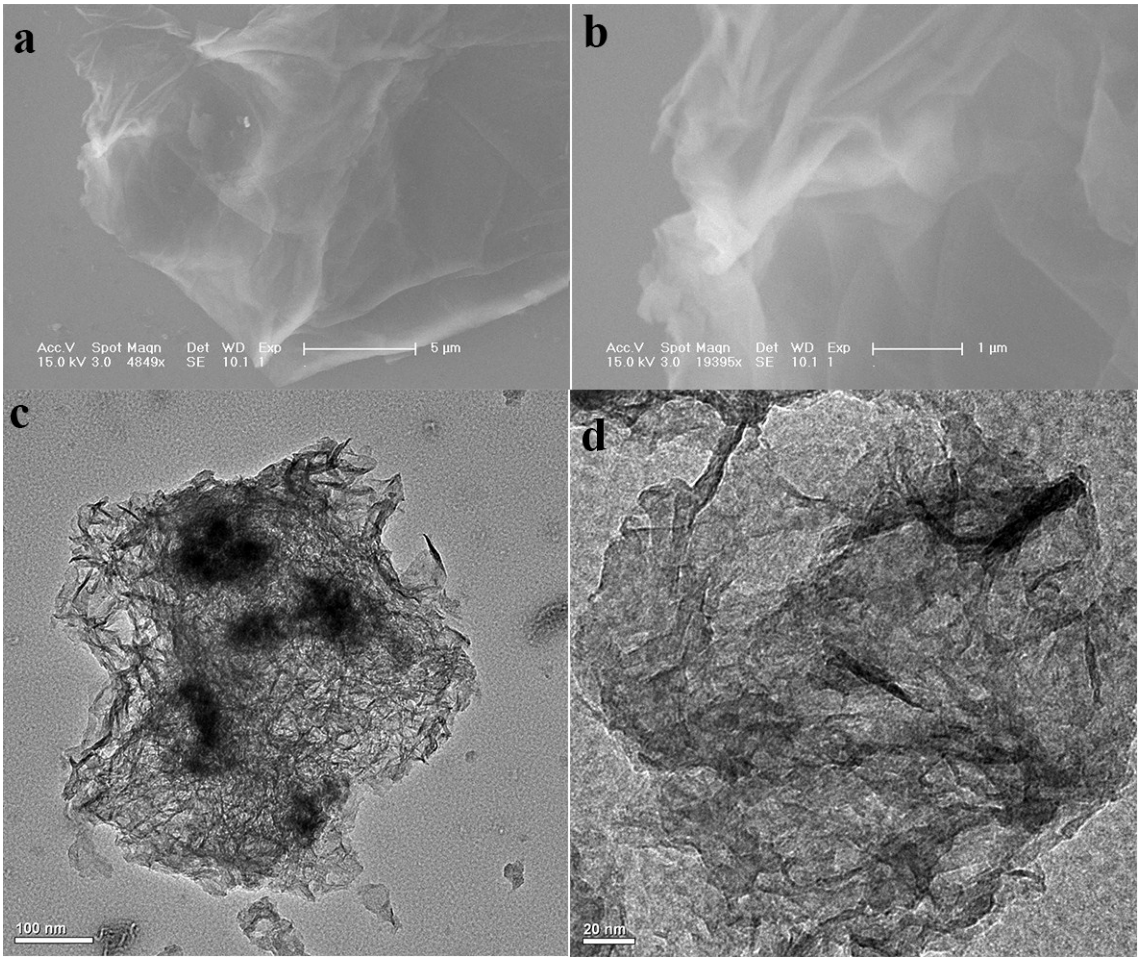

Fig. S1 SEM (a and b) and TEM (c and d) images for frehsh prepared CoP NS.

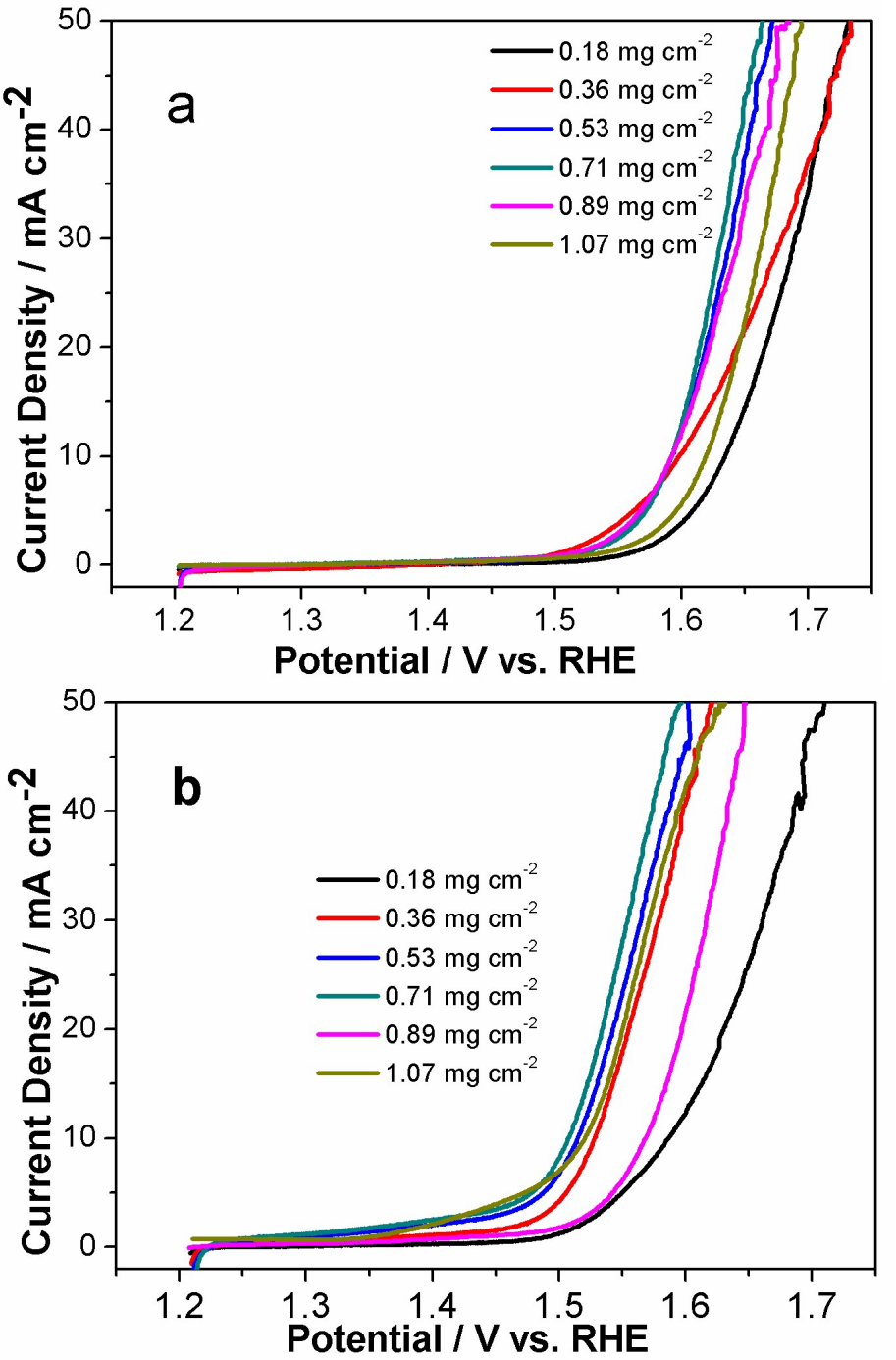

Fig. S2. Polarization curves of CoP NS (a) and CoP NS/C (b) in oxygen saturated 1 M KOH solution with different catalysts loading on GC; scanning rate was 5 mV s^{-1} and Potentials were corrected with iR drop.

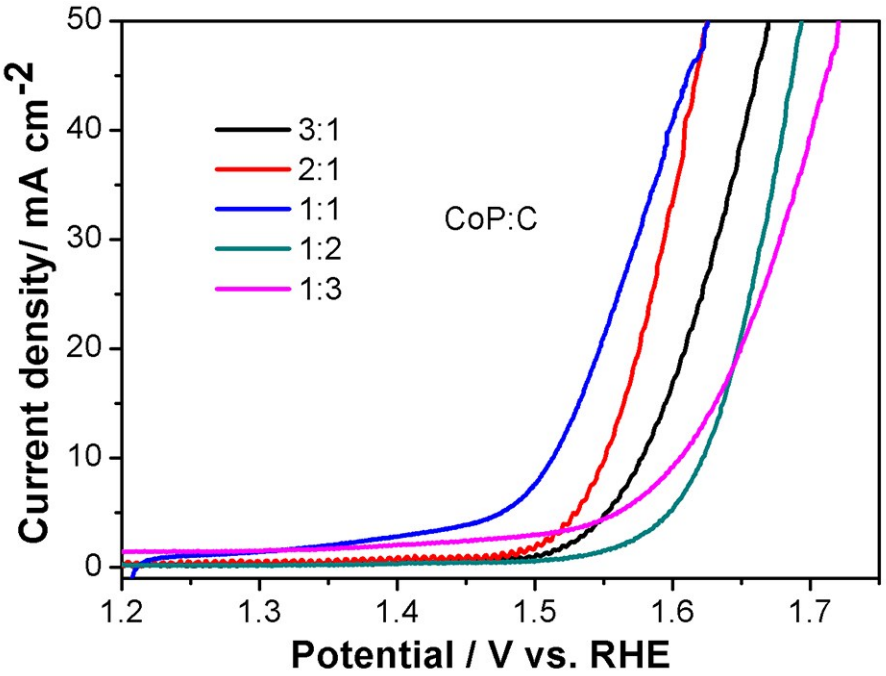

Fig. S3 OER performance for CoP NS/C with different CoP NS and C mass ration in 1 M O_2-saturated KOH. The scan rate was 5 mV s^{-1} and catalysts loading was 0.71 mg cm^{-2}.

As can be seen from the above figure, mass ratio effect of CoP : C on water splitting exhibits a volcano-shaped curve, with the optimized ratio located at 1:1. While mass ratios at >1 provide insufficient electron conductivity, the values at <1 supply insufficient catalytic sites for the reaction, thus, leading to inferior performances on both ends. Base the above results, we have chosen the ratio at 1:1 for all following measurements.

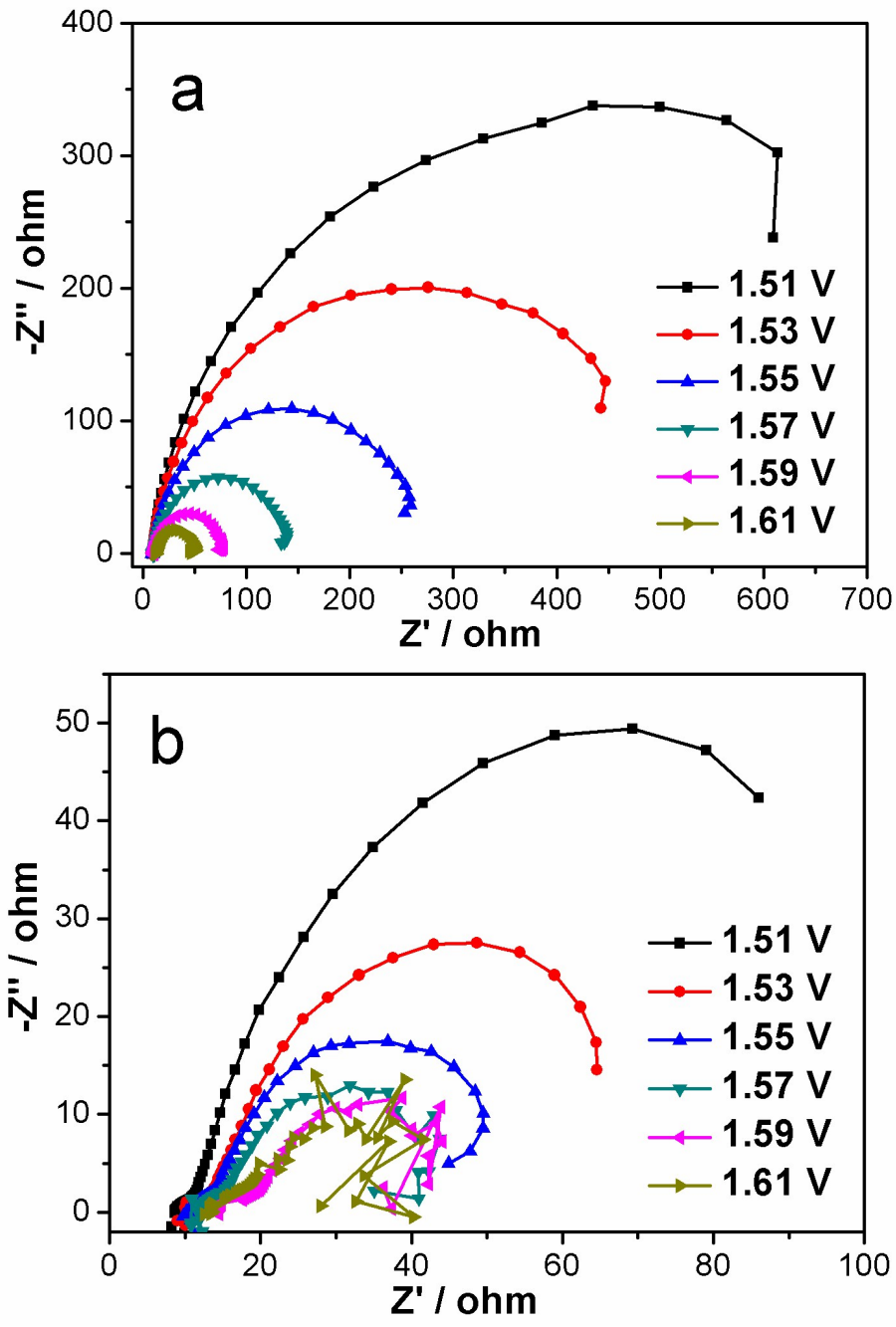

Fig. S4 Nyquist plots of the CoP NS (a) and CoP NS/C (b) in oxygen saturated 1 KOH solutions.

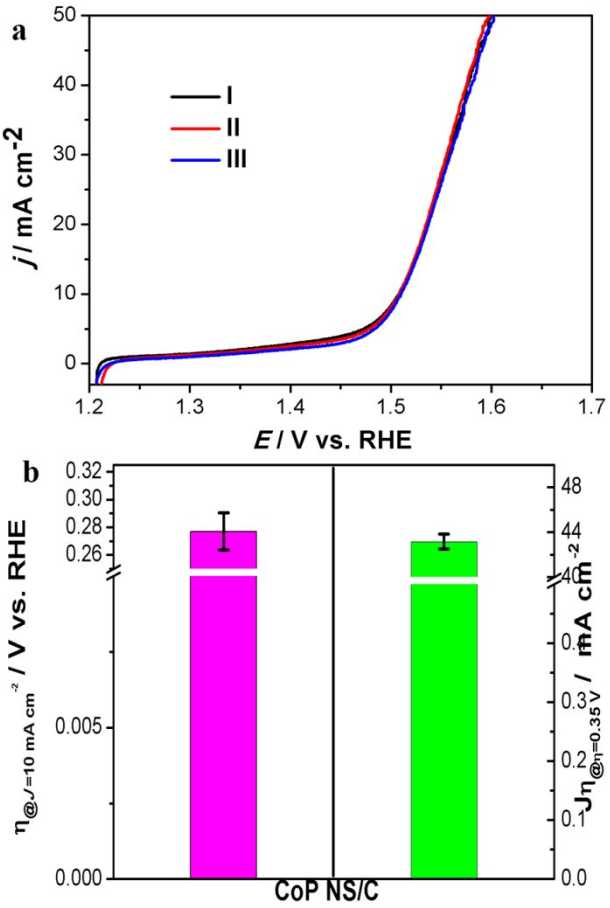

Fig. S5 a) OER performance for CoP NS/C (mass ration, 1:1) in 1 M O_2-saturated KOH solution. The scan rate was 5 mV s^{-1} and catalysts loading was 0.71 mg cm^{-2}. I, II and III represent three independent measurements respectively; b) The Over-potential required for J =10 mA cm^{-2} and current density at η = 0.35 V. The error bar represents the range of results from three independent measurements.

the electrochemical tests for each catalyst were repeated for at least three times, where high reproducibility was acquired. For instance, Fig. S5a presents three independent measurements of CoP NS/C (mass ration, 1:1), where the three polarization curves overlap almost perfectly. From Fig. S5 b, it is observed that the error was in allowance range area. Hence, we confirm that our results are credible and can be reproduced.

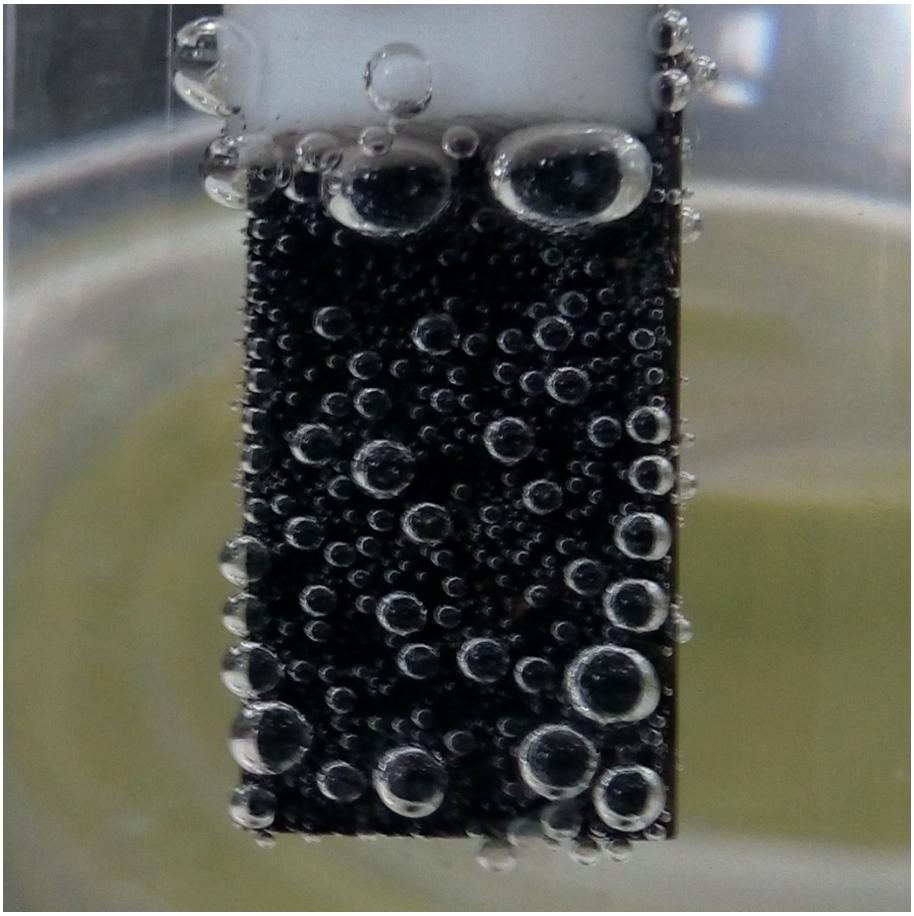

Fig. S6 Optical photograph showing the genration of oxygen bubbles on CoP NS/C supported on glass carbon sheets during FE test.

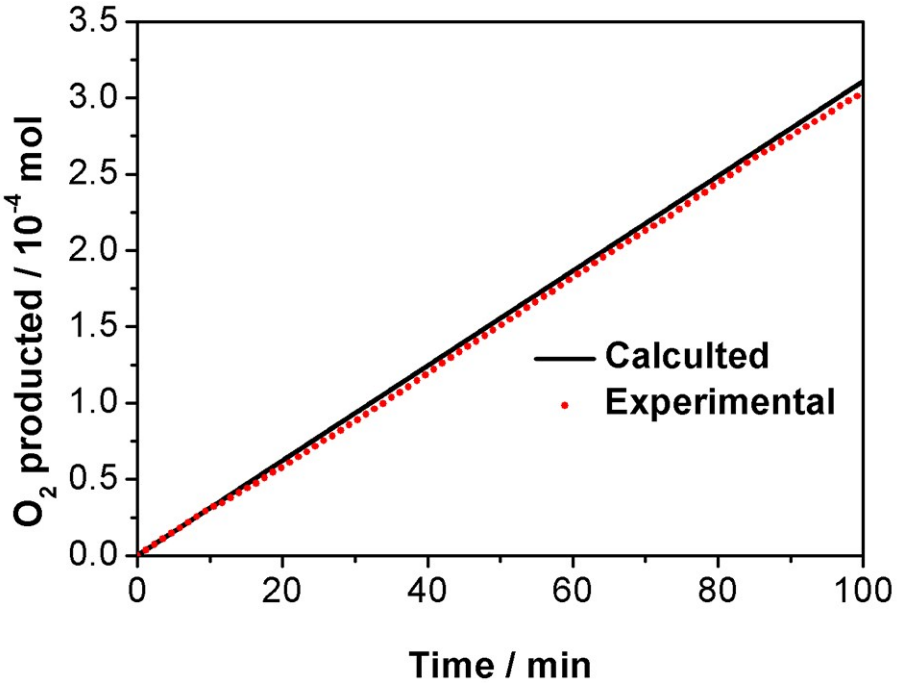

Fig. S7 Calculated versus actual oxygen production catalyzed by CoP NS/C at a constant oxidative current of 10 mA cm^{-2} in 1 M KOH for 100 min.

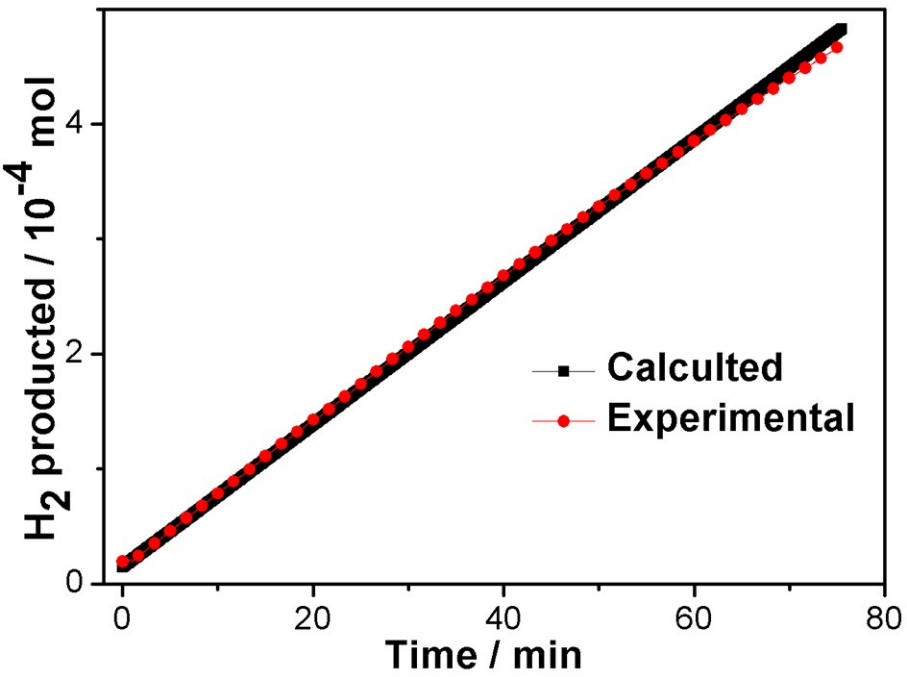

Fig. S8 Calculated versus actual hydrogen production catalyzed by CoP NS/C at a constant oxidative current of 10 mA cm^{-2} in 1 M KOH for 80 min.

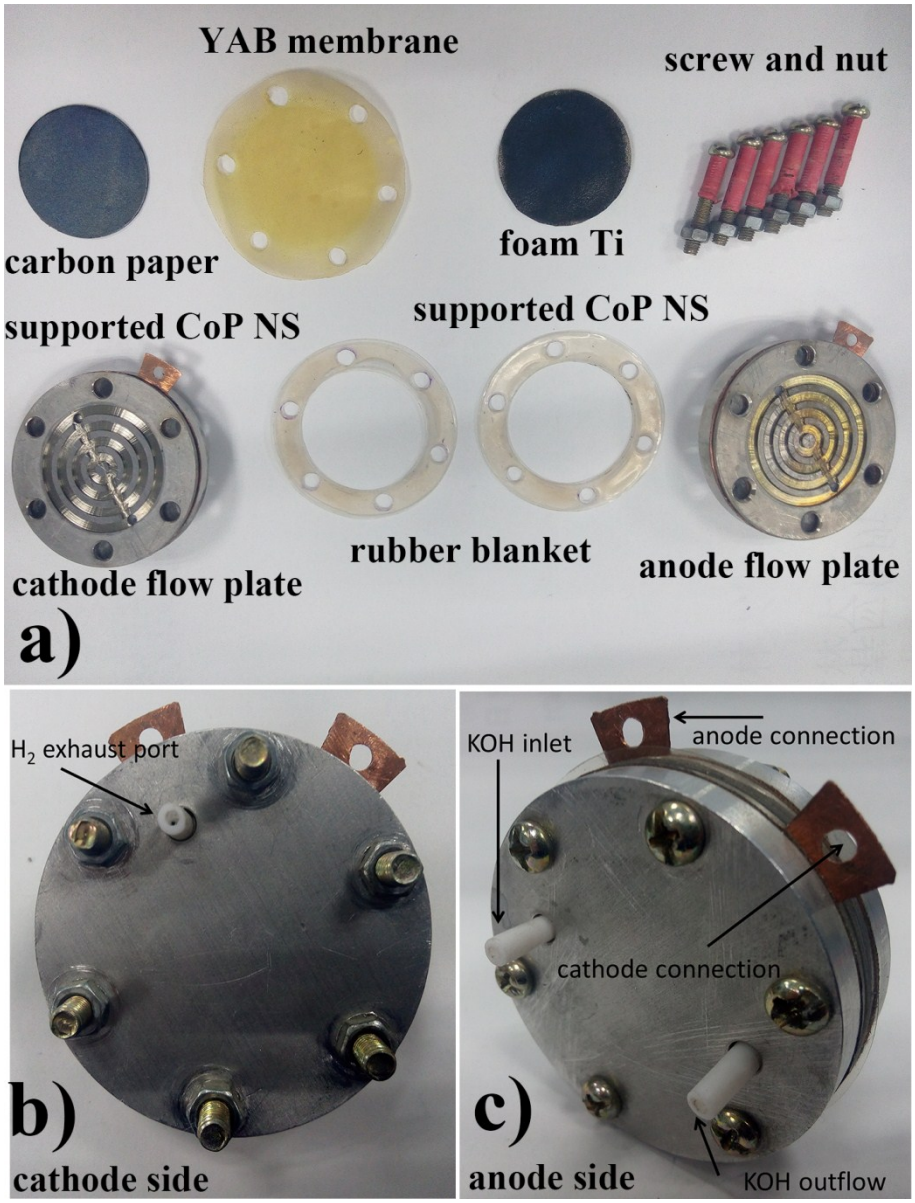

Fig. S9 Potograph of a) AEMWE cell configuration, b) cathode side and c) anode side of the electrolytic cell.

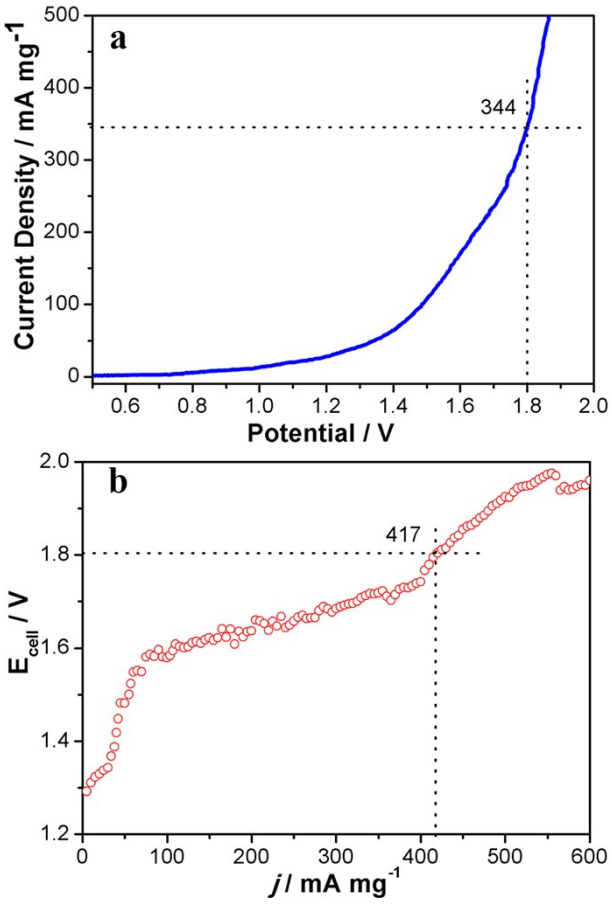

Fig. S10 Current-potential (a) response of the electrolyzer using CoP NS as catalyst both for OER and HER in 1 M KOH solutions and (b) polarization curve for a real water electrolysis cell normalize to mass activity derive from **Fig. 5a** and **Fig. 5c**.

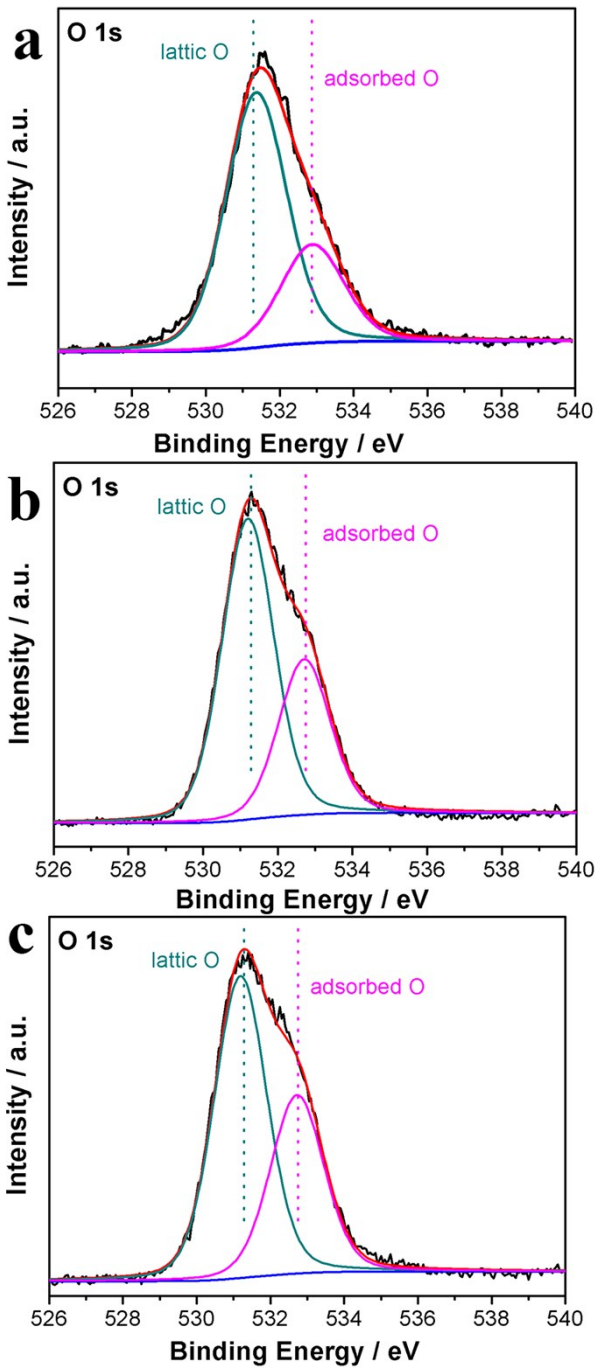

Fig. S11 Comparison the high-resolution XPS patterns for O 1s of the fresh prepared CoP NS (a) with the CoP NS that after electrolysis on cathode HER side (b) and anode OER side (c).

References

1. P. Jiang, Q. Liu, C. Ge, W. Cui, Z. Pu, A. M. Asiri and X. Sun, *J. Mater. Chem. A*, 2014, **2**, 14634-14640.
2. Q. Liu, J. Tian, W. Cui, P. Jiang, N. Cheng, A. M. Asiri and X. Sun, *Angew. Chem. Int. Ed.*, 2014, **53**, 6710-6714.
3. Y. Leng, G. Chen, A. J. Mendoza, T. B. Tighe, M. A. Hickner and C. Y. Wang, *J. Am. Chem. Soc.*, 2012, **134**, 9054-9057.
4. F. Song and X. Hu, *Nat. Commun.*, 2014, **5**, 4477.
5. Y. Gorlin and T. F. Jaramillo, *J. Am. Chem. Soc.*, 2010, **132**, 13612–13614.
6. T. Y. Ma, S. Dai, M. Jaroniec and S. Z. Qiao, *Angew. Chem. Int. Ed.*, 2014, **53**, 7281-7285.
7. H. Jin, J. Wang, D. Su, Z. Wei, Z. Pang and Y. Wang, *J. Am. Chem. Soc.*, 2015, **137**, 2688-2694.
8. K. Fominykh, J. M. Feckl, J. Sicklinger, M. Döblinger, S. Böcklein, J. Ziegler, L. Peter, J. Rathousky, E.-W. Scheidt, T. Bein and D. Fattakhova-Rohlfing, *Adv. Funct. Mater.*, 2014, **24**, 3123-3129.
9. C. Zhu, D. Wen, S. Leubner, M. Oschatz, Wei Liu, Matthias Holzschuh, Frank, Simon, Stefan Kaskel and a. A. Eychmüller, *Chem Commun (Camb)*, 2015, **51**, 7851-7854.
10. Y. Liang, Y. Li, H. Wang, J. Zhou, J. Wang, T. Regier and H. Dai, *Nat. Mater.*, 2011, **10**, 780–786.
11. S. Mao, Z. Wen, T. Huang, Y. Hou and J. Chen, *Energy Environ. Sci.*, 2014, **7**, 609-616.
12. T. Y. Ma, S. Dai, M. Jaroniec and S. Z. Qiao, *J. Am. Chem. Soc.*, 2014, **136**, 13925-13931.
13. F. Song and X. Hu, *J. Am. Chem. Soc.*, 2014, **136**, 16481-16484.
14. H. Liang, F. Meng, M. Caban-Acevedo, L. Li, A. Forticaux, L. Xiu, Z. Wang and S. Jin, *Nano letters*, 2015, **15**, 1421-1427.
15. H. Shi and G. Zhao, *J. Phys. Chem. C*, 2014, **118**, 25939-25946.
16. M. Gong, Y. Li, H. Wang, Y. Liang, J. Z. Wu, J. Zhou, J. Wang, T. Regier, F. Wei and H. Dai, *J. Am. Chem. Soc.*, 2013, **135**, 8452-8455.
17. D. Wang, X. Chen, D. G. Evans and W. Yang, *Nanoscale*, 2013, **5**, 5312-5315.
18. Q. Liu, A. M. Asiri and X. Sun, *Electrochem. commun.*, 2014, **49**, 21-24.
19. M. Ledendecker, G. Clavel, M. Antonietti and M. Shalom, *Adv. Funct. Mater.*, 2015, **25**, 393-399.
20. J. Wang, H. X. Zhong, Y. L. Qin and X. B. Zhang, *Angew. Chem. Int. Ed.*, 2013, **52**, 5248-5253.
21. J. Chang, Y. Xiao, M. Xiao, J. Ge, C. Liu and W. Xing, *ACS Catalysis*, 2015, **5**, 6874-6878.
22. Y. Yang, H. Fei, G. Ruan and J. M. Tour, *Adv. Mater.*, 2015, **27**, 3175-3180.
23. C. Tang, Z. Pu, Q. Liu, A. M. Asiri and X. Sun, *Electrochimica Acta*, 2015, **153**, 508-514.
24. C. Tang, Z. Pu, Q. Liu, A. M. Asiri, Y. Luo and X. Sun, *Int. J. Hydrogen Energy* 2015, **40**, 4727-4732.
25. C. Tang, N. Cheng, Z. Pu, W. Xing and X. Sun, *Angew. Chem. Int. Ed.*, 2015, **127**, 9483-9487.
26. L.-A. Stern, L. Feng, F. Song and X. Hu, *Energy Environ. Sci.*, 2015, **8**, 2347-2351.
27. J. Shi, Z. Pu, Q. Liu, A. M. Asiri, J. Hu and X. Sun, *Electrochimica Acta*, 2015, **154**, 345-351.
28. M. Ledendecker, S. Krick Calderon, C. Papp, H. P. Steinruck, M. Antonietti and M. Shalom, *Angew. Chem. Int. Ed.*, 2015, **127**, 12538-12542.
29. A. B. Laursen, K. R. Patraju, M. J. Whitaker, M. Retuerto, T. Sarkar, N. Yao, K. V. Ramanujachary, M. Greenblatt and G. C. Dismukes, *Energy Environ. Sci.*, 2015, **8**, 1027-1034.
30. H. Fei, Y. Yang, Z. Peng, G. Ruan, Q. Zhong, L. Li, E. L. Samuel and J. M. Tour, *ACS applied materials & interfaces*, 2015, **7**, 8083-8087.
31. X. Zou, X. Huang, A. Goswami, R. Silva, B. R. Sathe, E. Mikmekova and T. Asefa, *Angew. Chem. Int. Ed.*, 2014, **53**, 4372-4376.
32. J. Tian, Q. Liu, A. M. Asiri and X. Sun, *J. Am. Chem. Soc.* , 2014, **136**, 7587-7590.
33. M. Shalom, S. Gimenez, F. Schipper, I. Herraiz-Cardona, J. Bisquert and M. Antonietti, *Angew. Chem. Int. Ed.*, 2014, **53**, 3654-3658.
34. Z. Pu, Q. Liu, A. M. Asiri and X. Sun, *ACS Appl. Mater. Interfaces*, 2014, **6**, 21874-21879.
35. Y. Liang, Q. Liu, A. M. Asiri, X. Sun and Y. Luo, *ACS Catalysis*, 2014, **4**, 4065-4069.
36. M. Gong, W. Zhou, M. C. Tsai, J. Zhou, M. Guan, M. C. Lin, B. Zhang, Y. Hu, D. Y. Wang, J. Yang, S. J. Pennycook, B. J. Hwang and H. Dai, *Nat. Commun.*, 2014, **5**, 4695.
37. A. Han, S. Jin, H. Chen, H. Ji, Z. Sun and P. Du, *J. Mater. Chem. A*, 2014, **3**, 1941-1946.
38. S. Gu, H. Du, A. M. Asiri, X. Sun and C. M. Li, *Phys. Chem. Chem. Phys.*, 2014, **16**, 16909-16913.